Aquatic Sciences (2019) 81:58
https://doi.org/10.1007/s00027-019-0652-1

Aquatic Sciences

RESEARCH ARTICLE

A simple model for the numerical characterization of spatiotemporal variability in aquatic ecosystems

Rodrigo Gonzalez-Valencia[1] · Felipe Magaña-Rodriguez[1] · Armando Sepulveda-Jauregui[2,3] · Teresa Aguirrezabala-Campano[1] · Oscar Gerardo-Nieto[1] · Frederic Thalasso[1]

Received: 24 November 2018 / Accepted: 5 July 2019

Abstract

Aquatic ecosystems are subject to spatiotemporal variations that are important to quantify and understand for a proper assessment of their diversity and complexity. The objective of the present study was to develop a simple model that gives a numerical value to homogeneity and other spatiotemporal attributes for an easier analysis of aquatic ecosystem structure. The model allows for the comparison among different ecosystems, or different periods of time or zones of a given aquatic ecosystem. The model developed sets a numerical value to homogeneity, establishes the fraction of the ecosystem that contains a given percentage of the total amount of a compound, quantifies the fraction of the aquatic ecosystem in which no detectable levels of the measured compound are found, identifies the fraction of the ecosystem that represents an adequate habitat for a given process, and defines a simplified bidimensional vector of heterogeneity. This model is applicable to the two main maps used in the field of limnology: maps showing a particular parameter over two spatial dimensions, and maps showing a particular parameter over one spatial and one temporal dimension. The model was tested with different parameters obtained from three contrasting aquatic ecosystems, a highly polluted Mexican highland reservoir, a naturally acidic German bog lake, and a mesotrophic Patagonian lake.

Keywords Depth-space · Depth-time · Distribution · Homogeneity · Maps · Methane

List of symbols

λ_P	Dead area/section of parameter P
$\lambda_{P,X}$	Unidimensional (X) dead section of parameter P
$\Omega_{P,X,Y}$	Magnitude of the bidimensional (X, Y) vector of anisotropy for parameter P
$\omega_{P,X,Y}$	Direction of the bidimensional (X, Y) vector of anisotropy for parameter P
A	Grid cell area
A'	Cumulative normalized grid cell area
$A_P^{\%}$	Fraction of the map that contains a given percentage (superscript %) of parameter P
$A_{P,X}^{\%}$	Unidimensional (X) fraction of a profile, that contains a given percentage (superscript %) of parameter P
C_{CH4}	Concentration of disolved methane
C_{DO}	Concentration of dissolved oxygen
D	Depth
$E_{h,P}$	Relative absolute error of homogeneity factor for parameter P
F_P	Flux of parameter P
h_P	Homogeneity factor of parameter P
$h_{P,X}$	Unidimensional (X) homogeneity factor of parameter P
$K_{S,CH4}$	Apparent affinity constant for methane
$K_{S,DO}$	Apparent affinity constant for dissolved oxygen
L	Length
L'	Cumulative normalized length
MP	Methanotrophic potential
M_P	Magnitude of parameter P present in grid cell area
M'_P	Cumulative normalized magnitude of parameter P

Electronic supplementary material The online version of this article (https://doi.org/10.1007/s00027-019-0652-1) contains supplementary material, which is available to authorized users.

✉ Frederic Thalasso
thalasso@cinvestav.mx

[1] Departamento de Biotecnología Y Bioingeniería, Cinvestav, Av. IPN 2508, 07360 Mexico City, DF, Mexico

[2] Department of Experimental Limnology, Leibniz Institute of Freshwater Ecology and Inland Fisheries, Alte Fischerhütte 2, 16775 Stechlin, Germany

[3] Present Address: University of Magallanes, Faculty of Sciences, Av. Bulnes 01855, Punta Arenas, Chile

Published online: 19 July 2019

$N_{P,X}$	Unidimensional (X) magnitude of parameter P
$N'_{P,X}$	Unidimensional (X) cumulative normalized magnitude of parameter P
t	Time

Abbreviations

CV	Coefficient of variation
DO	Dissolved oxygen
IC	Inorganic carbon
LF	Lake Grosse Fuchskuhle
LG	Lake Guadalupe
LG#	Sampling sites in LG (1–8)
LH	Lake Hambre
MAD	Median absolute deviation
NHM	Numerical homogeneity model
RWCS	Relative water column stability
TC	Total carbon
TN	Total nitrogen
TOC	Total organic carbon

Introduction

Aquatic ecosystems are subject to variations on different scales and dimensions, i.e. across diel cycle and seasons (temporal), or depth- and lengthwise (spatial), collectively referred to as spatiotemporal variations. For instance, thermal stratification promotes strong vertical gradients of dissolved oxygen (DO), methane (CH_4), carbon dioxide (CO_2) concentration, and other physicochemical parameters. Depending on the mixing regime (Hutchinson and Löffler 1956; Imboden and Wüest 1995), the water column stratification often disappears, once or several times per year, thus adding a temporal dimension to vertical variations. Aquatic ecosystems are also subject to longitudinal variability caused by interactions with the contiguous terrestrial ecosystem, river inlets, and lateral transport, but also caused by zonation, morphology, and geology of the ecosystem (Giling et al. 2017; Hofmann 2013; Wik et al. 2013). These spatiotemporal variations are often radical, transitioning from oxic to anoxic, mesophilic to psychrophilic or photic to aphotic conditions, among others, in relatively short distances or timeframes.

Evidently, spatiotemporal variability has a large impact on the biogeochemical processes occurring in aquatic ecosystems. This can be illustrated by the CH_4 emissions to the atmosphere of which aquatic ecosystems have been identified as a major global source (Bastviken et al. 2004). Overall, CH_4 emissions depend on the complex balance between methanotrophy and methanogenesis; i.e., CH_4 oxidation and production, respectively, which in turn depend on the environmental conditions found in the aquatic ecosystem. Since CH_4 diffusive emissions are proportional to the surface dissolved CH_4 concentration (Weber et al. 2019), they will be the result of the biological and transfer processes occurring in the sediments, along the entire water column (Sepulveda-Jauregui et al. 2018a), and potentially along longitudinal gradients caused by lateral transport (Hofmann 2013). Ebullitive emissions, will depend mostly on the conditions found in the sediments as well as gas/water mass transfer during bubble migration to the surface, which also depends on the conditions found along the water column (Delwiche and Hemond 2017). Other illustrative examples are primary production and heterotrophic respiration; the first depends mostly on light penetration and CO_2 concentration, and is therefore subject to high spatiotemporal variability limited to the upper layers of the water column (Pannard et al. 2008; Winder and Hunter 2008), while the latter depends on organic matter and DO concentrations (Jane and Rose 2018).

Taking into consideration the spatiotemporal variability of aquatic ecosystems is beneficial to reach a proper assessment of the diversity and complexity of these environments. Through the recent development of high-frequency sensors at an affordable cost, measurements can be now distributed through time and/or space at high resolution, for the assessment of variability in one or more dimensions. The large datasets generated are usually presented in the form of contour or heat maps, which allow for a clear visual representation of the distribution of the studied parameters. Two distinct heat maps are typically used, maps showing a particular parameter over two space dimensions, hereafter termed "space–space maps", and maps displaying a particular parameter over one time and one space dimension, hereafter termed "space–time maps". Space–space maps may represent a parameter distribution over a vertical section of the aquatic ecosystem (Hofmann 2013; Steinle et al. 2015; Watkins et al. 2015) or over the surface area of the ecosystem (Gerardo-Nieto et al. 2017; Kaizu et al. 2011), while space–time maps usually represent a parameter profile over the water column and a given period of time (Bellido et al. 2013; Hofmann et al. 2010; Murase et al. 2005; Striegl and Michmerhuizen 1998). These maps facilitate a qualitative awareness of spatiotemporal distributions, identify hot- and cold-spots (Bagstad et al. 2017; Giling et al. 2017), and elucidate the overall structural properties of ecosystems at different scales (He et al. 2002).

Going further, a quantitative approach to the structural properties of an aquatic ecosystem assigns a numerical value to the spatiotemporal variations of a given parameter in space–space or space–time distributions. There is an extensive literature on methods to assess spatiotemporal distributions in a diversity of ecosystems. These methods allow for the treatment of occurrence (based on magnitude) or abundance (based on presence–absence) datasets, and for the determination of specific properties of the studied ecosystem. The main methods have been listed

and compared (Fraterrigo and Rusak 2008; Legendre and Fortin 1989; Veldtman 2005). Among them, Moran's I (Moran 1950), Geary's C (Geary 1954), K-means (Thah and Sitanggang 2016), semivariogram (Matheron 1963) or spatially stratified heterogeneity (Wang et al. 2016) methods, allow for the numerical quantification of heterogeneity as well as for the determination of structural parameters, such as patchiness or anisotropy (Legendre and Fortin 1989; Rosenberg 2000). However, these methods are sophisticated and complex, they often require significant computing effort, they are better adapted to large scale with space–space dimensions, and generally not well-adapted for the characterization of continuous variations of environmental properties (Gustafson 1998). Although the listed methods, and other such as spectral or wavelet analysis, have been applied to continuous environmental data, their focus has been segregation of patterns in large datasets (Legendre and Fortin 1989), with a substantial computational effort (Li 1995; Rajala et al. 2018).

Thus, there is still a demand for simple numerical methods to characterize spatiotemporal dispersion of environmental parameters in aquatic ecosystems. Gonzalez-Valencia et al. (2016) suggested a numerical model to describe spatial variations of CH_4 emissions from landfills, that can be easily applied with slight computing effort. The objective of this study was to adapt and expand the previously reported model, called numerical homogeneity model (NHM) to describe and quantify spatiotemporal variations of environmental parameters in aquatic ecosystems, with the attributes hereafter described. First, the NHM should be easily applicable with no specialized background on numerical methods and with little computing effort. Second, the model should give a numerical value to the spatiotemporal variations of any intensive or extensive property. Third, the NHM should be applicable to continuous or discrete data. Fourth, the model should be applicable to describe spatiotemporal variations of a given parameter over one time, one space, two space–time or two space–space dimensions. Fifth, the NHM should support comparisons among ecosystems, as well as among periods of time or sections of a given ecosystem. Sixth, preferably, the NHM should detect and quantify regions with a specific structural property, including but not limited to the fraction of the ecosystem that contains a certain level of a given parameter, and to quantify possible dead volumes, i.e., the fraction that contains no detectable level of the measured parameter. Seventh, the NHM should enable the combination of the structural properties of several parameters, to determine the available habitat for a given biogeochemical process; e.g., light and CO_2 concentration for primary production, CH_4 and DO concentration for oxic methanotrophy, or organic matter and DO concentration for heterotrophic respiration. In this work a numerical homogeneity model was developed and tested with data obtained in different lakes and reservoirs.

Numerical homogeneity model

Our NHM was developed to give a numerical value to homogeneity and spatiotemporal variation attributes represented in space–space or space–time heat maps. Space–space maps can be a vertical section of the aquatic ecosystem; i.e., depth-length maps, which allow for the characterization of the water column homogeneity along a longitudinal transect. Space–space maps can also represent the surface of the aquatic ecosystem, to test for instance spatial distribution of gas emissions, or any horizontal section of the ecosystem to quantify the parameter distribution at a fixed depth. Space–time maps would generally represent the water column homogeneity along a period of time, although the space dimension might be any characteristic length.

The model first establishes a homogeneity factor (h_P) that gives a numerical value to the spatial distribution of a given parameter indicated by subscript P. For the determination of h_P, the heat map is partitioned into a grid of n sub-regions, each one corresponding to one parameter value ($P_{i=1,2,\ldots,n}$). It is important to note that each P value can be a measured parameter or a product of interpolated contour maps. Each P_i is associated with a grid cell area ($A_{i=1,2,\ldots,n}$) that can be constant in the case of interpolated maps or variable in the case of experimental data. In the case of space–space maps, A represents an actual area (m^2), whereas in the case of space–time maps, A is a mixed parameter with units of length–time, e.g., m d. Next, we multiply the parameter P_i by the corresponding A_i to obtain a quantity of the compound of interest, or the magnitude of any other variable, present in the grid cell ($M_{Pi=1,2,\ldots,n}$). We reorder the M_{Pi} subscripts so that $M_{P1} \geq M_{P2} \geq \cdots \geq M_{Pn}$, keeping for each M_{Pi} the corresponding A_i. We finally establish a cumulative normalized parameter M'_{Pj} (Eq. 1) that varies from 0 to 1, which is coupled to a cumulative normalized A' function (Eq. 2).

$$0 \leq M'_{Pj} = \frac{\sum_{i=1}^{j} M_{Pi}}{\sum_{1}^{n} M_{Pi}} \leq 1 \tag{1}$$

$$0 \leq A'_{j} = \frac{\sum_{i=1}^{j} A_i}{\sum_{1}^{n} A_i} \leq 1 \tag{2}$$

The spatial (space–space maps) or spatiotemporal (space–time maps) distribution of the parameter in the ecosystem is then obtained by graphing the pair (M'_j, A'_j), and the homogeneity of the parameter P distribution is given by

h_P (%; Eq. 3), which is represented by the hatched area in Fig. 1a.

$$0 \le h_P = \frac{1 - \int_0^1 M'_P dA'}{0.5} \cdot 100 \le 100\% \quad (3)$$

The significance of this quantity is that for a homogeneous distribution, $h_P = 100\%$, while for a nonhomogeneous distribution, $0 \le h_P < 100\%$. In Fig. 1a, presented as theoretical example, the straight line indicates the trend of M'_{P_j} that would be observed in a perfectly mixed water volume in the case of depth-space maps, or a perfectly mixed water column over a time interval in the case of depth-time maps ($h_p = 100\%$).

In addition, we define a second parameter that gives the percentage of the total space–space or space–time map that contains a given percentage of the total amount of the parameter P ($A_P^{\%}$). In $A_P^{\%}$, superscript % indicates the corresponding percentage, from 0 to 100%, of the parameter P. For example, in the case of a space–space map, A_{DO}^{80} is the percentage of the ecosystem section that contains 80% of the total dissolved oxygen (DO). It is worth mentioning that if a compound is absent in a section of the ecosystem, its corresponding A_P^{100} will be less than 100% (Fig. 1a). Therefore, the complementary fraction of A_P^{100}, i.e., $100 - A_P^{100}$, gives a new parameter that we define as the dead area (λ_P), which represents the percentage of the section area that does not contain a detectable amount of P. The parameters A_P^{100} and λ_P are dependent upon the lower limit of detection of the method used for P measurements and cannot be considered strictly as true characteristics of the ecosystem. However, if the lower limit of detection of the method is close to zero, little differences between λ_P and the actual dead section of the ecosystem is expected.

The model for the determination of h_P, $A_P^{\%}$, and λ_P is applicable to an entire aquatic ecosystem, as shown above, but also to a specific section of it, or even to a single time or space dimension. Consequently, it allows, for instance, to discriminate longitudinal and depth distributions in space–space maps, or depth and temporal distributions in space–time maps. When the NHM is used to establish a single dimension distribution, additional subscripts are added to the homogeneity parameters for clarity: (1) subscript D, when only referring to depth profiles, e.g., $h_{P,D}$, (2) subscript L, when only referring to longitudinal profiles, e.g., $A_{P,L}^{\%}$ and (3) subscript t, when only referring to temporal profiles, e.g., $\lambda_{P,t}$. It is worth mentioning that in the case of a single dimension analysis, each parameter P_i is not associated with a grid cell area ($A_{i=1,2,\ldots,n}$), as in two-dimensional analysis, but with a characteristic length ($L_{i=1,2,\ldots,n}$); i.e., distance or time between two measurements or two interpolated data. Similarly, $N_{P,X}$ replaces M_P in the single dimension analysis, which is obtained by multiplying the parameter by the characteristic length. Therefore, the procedure of data treatment is similar, except that Eq. (3) is replaced by Eq. (4).

$$0 \le h_P = \frac{1 - \int_0^1 N'_{P,X} dL'}{0.5} \cdot 100 \le 100\% \quad (4)$$

Thus, the model also allows the comparison between two single dimension distributions. For comparison, we suggest a new parameter which describes the overall heterogeneity ($\Omega_{X,Y}$; Eq. 5), where subscripts X and Y represent the space or time dimensions being compared, and where heterogeneity is considered as the complement of homogeneity; e.g., $100 - h_P$, expressed in percent. It is worth mentioning that the maximum value of $\Omega_{X,Y}$ is 141%, as a result of the square root of 20,000 when $h_{P,X}$ and $h_{P,Y}$ are 0%.

$$0 \le \Omega_{P,X,Y} = \sqrt{\left(100 - h_{P,X}\right)^2 + \left(100 - h_{P,Y}\right)^2} \le 141\% \quad (5)$$

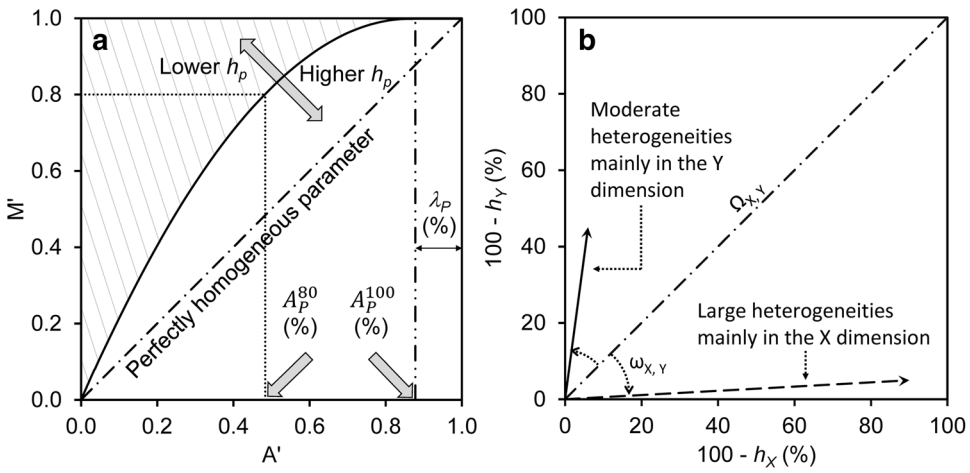

Fig. 1 **a** Example of a homogeneity graph showing the cumulative distribution of the M' parameter over A′ (solid line), the distribution that would be observed in a perfectly homogeneous system (dot-dash line), and a graphical representation of the determination of $A_P^{\%}$ and λ_P. The dashed area represents the integral of Eq. (3). **b** Theoretical representation of the simplified bidimensional vector of anisotropy

Additionally, we also define an angle ($\omega_{X,Y}$, expressed in degrees, Eq. 6) which represents the angle of $\Omega_{X,Y}$ with respect to a Y = X straight line (Fig. 1b). The Y = X line represents the direction in which both dimensions being compared have an equal heterogeneity, and therefore a $\omega_{X,Y}$ of − 45° means that heterogeneities are only observed in the X dimension, and conversely a $\omega_{X,Y}$ of + 45° means that heterogeneities are only observed in the Y dimension.

$$-45^\circ \leq \omega_{P,X,Y} = arcos\left(\frac{100 - h_{P,X}}{\Omega_{P,X,Y}}\right) - 45 \leq 45^\circ \quad (6)$$

The significance of $\Omega_{P,X,Y}$ and $\omega_{P,X,Y}$ is as follows; if depth and longitudinal homogeneities are combined, $\Omega_{P,L,D}$ will give the overall heterogeneities with consideration to longitudinal and depth axis, while $\omega_{P,L,D}$ will indicate the dominant direction of heterogeneities; i.e., negative values for longitudinal dominant heterogeneities, and positive values for vertical dominant heterogeneities (Fig. 1b). As such, a $\Omega_{L,D}$ of 120 and a $\omega_{P,L,D}$ of 0°, would indicate strong heterogeneities, equally distributed longitudinally and depthwise, while $\Omega_{P,L,D}$ of 10 and $\omega_{P,L,D}$ of 45°, would indicate relatively low heterogeneity but exclusively along the depth profile (Y-axis, Fig. 1b). Both $\Omega_{X,Y}$ and $\omega_{X,Y}$, are parameters that define the magnitude and direction of heterogeneities in the X–Y dimensions and can be considered, together, as a simplified bidimensional vector of anisotropy.

Materials and methods

Study site, monitoring stations, and dates

A 450-ha tributary reservoir called Lake Guadalupe (LG) was selected to test our numerical model (19.6310 N, 99.2567 W; Fig. S1). LG is a tropical highland reservoir that is 2240 m above sea level and 25 km northwest of Mexico City. Its general properties, as well as its limnological characteristics, have been reported previously (Gonzalez-Valencia et al. 2014; Sepulveda-Jauregui et al. 2013). Briefly, LG is dendritic, and its major axis runs southwest to northeast, where the dam is located (Fig. S1). In the western region, LG receives untreated urban wastewater discharges from three polluted tributary rivers, making LG a highly polluted ecosystem (Sepulveda-Jauregui et al. 2013). During the dry season (usually from October to June), LG serves as a water source, and a considerable decrease in its volume is usually observed. The lake has been previously characterized as monomictic, with a mixing period from November to April (Sepulveda-Jauregui et al. 2013). The present study was conducted from September to May to cover the period before, during, and after water column overturn, as well as from maximum to minimum reservoir volume. During this period, four sampling campaigns were conducted in September, December, March, and May.

Sampling methods

Eight equidistant monitoring stations were established along the longitudinal axis of LG, covering the fluvial, transitional, and lacustrine zones (Fig. S1). At each monitoring station, in situ water quality measurements were taken at 1-m depth intervals from the water surface to the bottom, i.e., temperature, pH, and DO concentration (C_{DO}), using a multiparametric probe (556 MPS, YSI, USA). At the same depths, dissolved CH_4 concentrations (C_{CH4}) were determined in situ using a previously described method based on headspace equilibration by infrared tunable diode laser absorption spectroscopy (Sepulveda-Jauregui et al. 2012). At each location and depth, water samples were taken with a horizontal 2.2-L Van Dorn bottle (WILDCO, USA). Water samples were transferred to polypropylene containers and handled using standard methods (APHA 2012). After transfer to the laboratory, the total carbon (TC), inorganic carbon (IC), total organic carbon (TOC), and total nitrogen (TN) were measured using a total C and N analyzer (Shimadzu TOC-V_{CSN} + TN1 module, Shimadzu, Mexico). Superficial and bottom water temperatures were measured every 30 min, during the complete sampling period, at three locations (LG1, LG4, and LG6; Fig. S1) using temperature loggers (HR, Thermotracker, Mexico) with 0.1 °C resolution. Water density values derived from the superficial and bottom water temperatures were used to determine the relative water column stability (RWCS; Padisák et al. 2003). If the RWCS was higher than 56.5, the lake was considered fully stratified, if it was less than 16.3, it was considered fully mixed, and at an intermediate RWCS value, the lake was considered partially stratified (Branco et al. 2009).

Space–space and space–time mapping

First, we used the data collected in LG, at all depths and locations, to elaborate vertical section maps. In complement, to test our numerical model with surface heat maps, we processed CH_4 flux data previously reported (Gerardo-Nieto et al. 2017) from the small, round-shaped, subantarctic Lake Hambre (LH; 53.6035S, 70.9525W), a mesophilic lake located 50 km south of Punta Arenas, Chile. Similarly, to test our numerical model with space–time heat maps, we used C_{DO} and C_{CH4} data previously reported by Sepulveda-Jauregui et al. (2018b) that were obtained from Lake Grosse Fuchskuhle (LF; 53.1054N, 12.9846E), which is a small, naturally acidic bog lake located in a forested area of the Mecklenburg-Brandenburg Lake District in north-eastern Germany. This lake was artificially divided three decades ago into two distinctive sections, northeast and southwest.

We used data collected over 1-year, from the northeast section, from August 2014 until July 2015.

Multiparametric estimations for process prediction

The NHM allows to combine the structural properties of several combined parameters for predictive purposes. To test that capability of the NHM, we combined C_{DO} and C_{CH4} data from LG and LF to estimate the methanotrophic potential (MP; %). Each C_{DO} and C_{CH4} measurements (same location and same depth) were combined according to a double Monod model (Segers 1998; Eq. 7);

$$MP = 100 \cdot \frac{C_{CH4}}{K_{S,CH4} + C_{CH4}} \cdot \frac{C_{DO}}{K_{S,DO} + C_{DO}} \quad (7)$$

where MP is the methanotrophic potential which represents the percentage of the maximum methanotrophic rate that would be observed with no C_{DO} and C_{CH4} limitations, and $K_{S,CH4}$ and $K_{S,DO}$ are the apparent affinity constants, for CH_4 and DO, respectively, and with respective values of 0.110 and 0.624 mg L^{-1} (Martinez-Cruz et al. 2015). Once MP values were determined for each sampling point, heat maps were generated from data interpolation and processed with the NHM.

Statistical analyses, mapping, and error determination

In all cases, the measured parameters were used to establish maps from data interpolation using Surfer 11.0 software (Golden Software, USA). Selection of the best interpolation method, among inverse distance to a power, Kriging, minimum curvature, natural neighbour, nearest neighbour, radial basis function, and modified Shepard's method all of them included in the Surfer software, was based on two criteria: the mean absolute error and the mean bias error (Willmott and Matsuura 2006). The maps produced were used to test the NHM. We also estimated the impact of sampling density on NHM, using the vertical section maps of C_{DO} and C_{CH4}, in LG. With that purpose, we produced reduced datasets by eliminating a given number of profiles or a given number of depth data. Each combination of reduced dataset was tested; i.e., C(n, k), where n is the total number of profiles or depths measured, and k is the number of profiles or depths considered in the reduced dataset. For each combination, a map was generated by interpolation and the factor h was determined. All h_P determined for a given (n, k) were averaged, compared to the original h_P of the complete dataset, and the relative absolute error was determined. It is worth mentioning that the reduced datasets obtained by reduction of the number of profiles or depths were treated separately to segregate both effects. Additionally, we numerically determined the impact of outliers on NHM parameter h_P, the coefficient of variation (CV) defined as the ratio between the standard deviation and the mean, and the median absolute deviation (MAD). The latter was performed by simulating a set of 300 data with normal distribution and adding an increasing percentage of outliers from 0 to 5%, 10 times higher than the mean of the dataset. The tests for sampling density and outliers were performed in MATLAB (R2015a, Mathworks Inc.).

Results and discussion

DO and C_{CH4} concentrations in LG

According to the water column temperature (Fig. S2), the lake was fully mixed from November until March. Figure 2 shows the vertical section maps of C_{DO}, which ranged from < 0.01 (lower limit of detection) to 6.72 mg L^{-1}, observed in the fluvial zone during winter (December), and was below the saturation concentration of 7.34 mg L^{-1} that was calculated from an atmospheric pressure of 0.77 atm and a superficial water temperature of 17.4 °C (Meteored 2016). Most of the water column was anoxic, and the average C_{DO} over the entire transect were 0.51, 0.37, 0.85, and 0.66 mg L^{-1} in September, December, March, and May, respectively. An oxycline was observed in all seasons, at a depth that varied from 0.5 m in December at LG1 to 4 m in March at LG4. In December, a longitudinal gradient of C_{DO} was observed from the fluvial to the lacustrine zones. These relatively low C_{DO} were a result of wastewater discharges that have previously been reported (Gonzalez-Valencia et al. 2014; Sepulveda-Jauregui et al. 2013).

Figure 3 presents vertical section maps of C_{CH4} that show a clear stratification in all seasons except December, and with a methanecline observed at the same depths as the oxycline. Depth gradients of dissolved CH_4 are a common feature of stratified lakes (Encinas Fernandez et al. 2014; Striegl and Michmerhuizen 1998). A negative relationship was observed between C_{CH4} and C_{DO}, with high C_{CH4} levels where low C_{DO} were observed, which suggests that there is an interaction between these compounds; i.e., the presence of DO promotes CH_4 oxidation (Sepulveda-Jauregui et al. 2018b). C_{CH4} levels varied over four orders of magnitude, from 0.007 to 13.55 mg L^{-1}, observed respectively in March at the epilimnion and in May at the hypolimnion. The average C_{CH4} concentrations over the entire transect were 2.09, 2.06, 1.43, and 3.23 mg L^{-1} in September, December, March, and May, respectively. The CH_4/DO molar ratio over the entire water column ranged from 2.86 in March to 8.39 in May. Because the molar ratio of methanotrophy is 0.5 mol of CH_4 oxidized per mole of oxygen, the observed CH_4/DO molar ratio indicates that at the reservoir scale, CH_4 was in

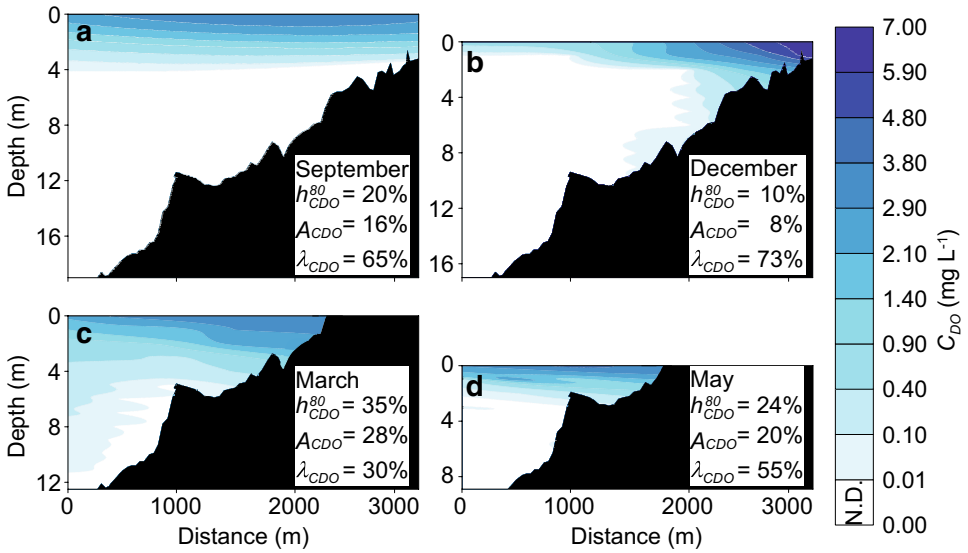

Fig. 2 Heat maps and NHM parameters of dissolved oxygen (C_{DO}) concentrations in Lake Guadalupe. **a** September, **b** December, **c** March, and **d** May. ND: not detected (DO < 0.01 mg/L). Black area represents bathymetry data

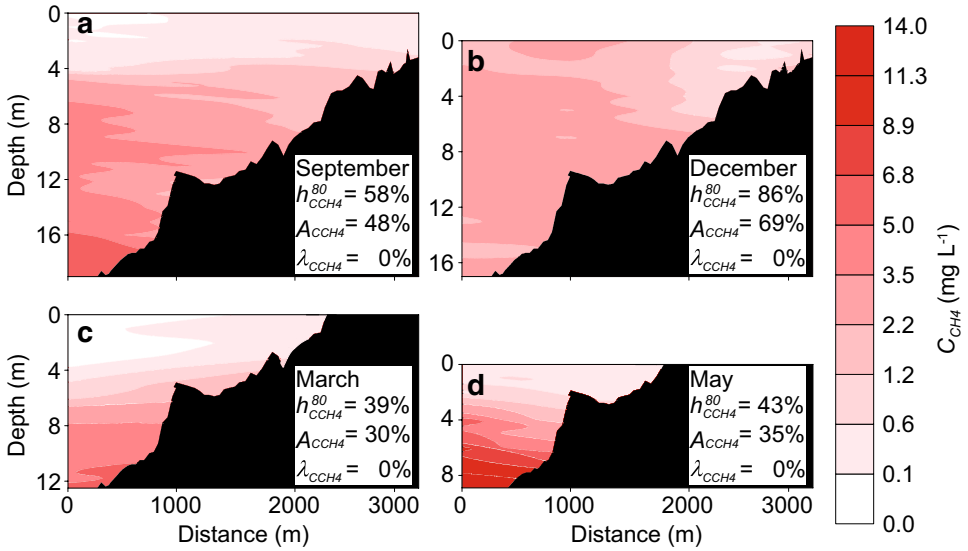

Fig. 3 Heat maps and NHM parameters of dissolved methane (C_{CH4}) concentrations in Lake Guadalupe in **a** September, **b** December, **c** March, and **d** May. Black area represents bathymetry data

excess, so DO was the limiting factor for CH_4 oxidation in most of the water column in all seasons.

Two-dimensional analysis

Figure 4 shows the spatial distributions of C_{CH4} and C_{DO} over LG transect, which confirms that by graphing the pair (M'_j, A'_j), the NHM gave in all cases an asymptotic shape that allows to visualize the homogeneity, and to quantify h_P, $A_P^{\%}$, and λ_P. In all seasons, C_{DO} was heterogeneously distributed, with h_{CDO} ranging from 10 to 35% and A^{80}_{CDO} ranging from 8 to 28% (Table 1), so during the most heterogeneous period, 8% of the lake section contained 80% of the total DO. In addition, because of a clear, anoxic section in the water column, A^{100}_{CDO} ranged from 27 to 70%, indicating a range of dead section for DO (λ_{CDO}) of 30 to 73%, i.e., the percentage of the reservoir section that could be considered anoxic. C_{CH4} was more homogeneously distributed than DO in all seasons, with h_{CCH4} ranging from 39 to 86% and A^{80}_{CCH4} ranging from 30 to 69% (Table 1). h_{CDO} and A^{80}_{CDO} were inversely proportional to h_{CCH4} and A^{80}_{CCH4}, respectively. This was particularly clear in December when the water column was well mixed, with the highest h_{CCH4} and A^{80}_{CCH4} and the lowest h_{CDO} and A^{80}_{CDO}, among seasons. In contrast, in March, the C_{DO} and C_{CH4} had similar distributions, which corresponded to the maximum h_{CDO} and A^{80}_{CDO} and the minimum h_{CCH4} and A^{80}_{CCH4}. Therefore, the spatial distributions of C_{CH4} and C_{DO} were linked, and a more homogeneous distribution of C_{CH4} promoted a more heterogeneous DO distribution, and vice versa. The correlation observed between

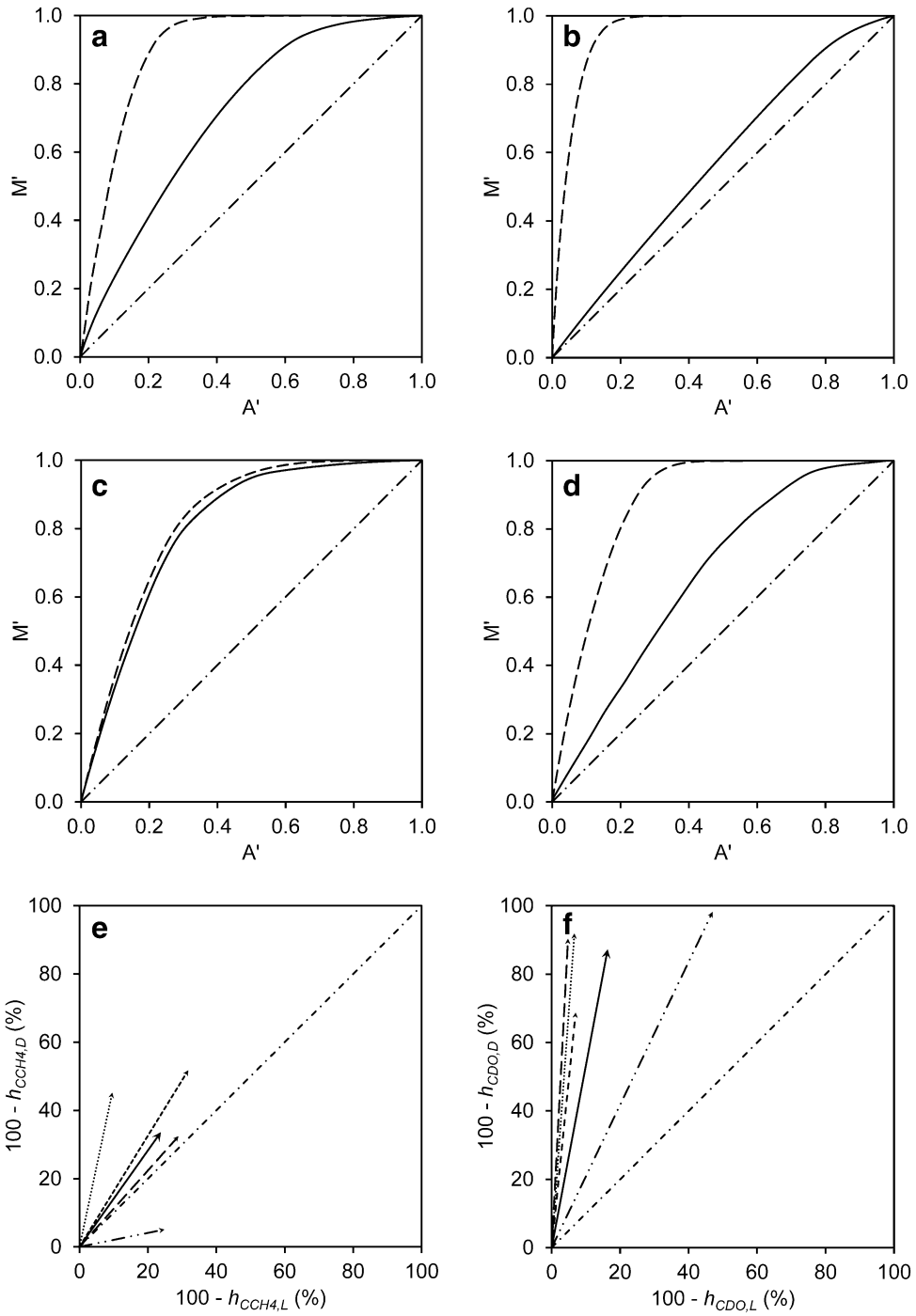

Fig. 4 Homogeneity graphs of dissolved methane (C_{CH4}; solid lines) and dissolved oxygen (C_{DO}; dashed lines) concentrations over the entire transect of Lake Guadalupe in **a** September, **b** December, **c** March, and **d** May. Simplified bidimensional vector of anisotropy in September (long-dashed line), December (dot-dot-dash line), March (short-dashed line), May (dotted line) and mean vector (solid line) for C_{CH4} (**e**) and C_{DO} (**f**)

h_{CDO} and h_{CCH4} indicates that both compounds were linked through methanotrophy; i.e., a higher h_{CDO} and A^{80}_{CDO} resulting in higher DO availability for methanotrophy and CH_4 oxidation, resulting in lower h_{CCH4} and A^{80}_{CCH4}, and reciprocally. Thus, the effects of stratification and mixing regime on the NHM parameters are complex and no direct link between them can be established. Indeed, the NHM in LG showed that mixing, observed in December, promoted the homogeneity of C_{CH4} but suppressed the homogeneity of C_{DO}. This observation suggests that NHM cannot be considered as an indicator of the stratification.

A two-dimensional, depth-length analysis was also performed from TOC, IC, and TN concentration data in LG, and Table 1 shows the h_P, $A^{\%}_P$, and λ_P determined. These three parameters were more homogeneously distributed than C_{CH4} and C_{DO}. The h_{TOC} ranged from 85% in December to 99% in March, and the spatial distribution of IC ranged from a h_{IC} of 50% in September to 99% in March. The lower h_{IC} observed

Table 1 Homogeneity parameters (h_P and A_P^{80}) and mean concentrations of several parameters in Lake Guadalupe at different times

	Parameter	September	December	March	May
CH_4	h_{CCH4} (%)	58	86	39	43
	A_{CCH4}^{80} (%)	48	69	30	35
	Mean conc. (mg L^{-1})	2.09 (1.56)	2.06 (0.59)	1.43 (1.70)	3.23 (3.60)
DO	h_{CDO} (%)	20	10	35	24
	A_{CDO}^{80} (%)	16	8	28	20
	Mean conc. (mg L^{-1})	0.52 (0.96)	0.37 (1.06)	0.86 (1.08)	0.66 (1.07)
TOC	h_{TOC} (%)	90	85	99	91
	A_{TOC}^{80} (%)	75	72	80	75
	Mean conc. (mg L^{-1})	11.16 (1.98)	27.4 (7.44)	26.65 (0.36)	21.1 (3.15)
IC	h_{IC} (%)	50	71	99	93
	A_{IC}^{80} (%)	42	59	80	76
	Mean conc. (mg L^{-1})	5.78 (6.26)	11.25 (5.74)	26.65 (0.42)	31.47 (3.92)
TN	h_{TN} (%)	95	85	98	97
	A_{TN}^{80} (%)	77	73	79	79
	Mean conc. (mg L^{-1})	1.95 (0.17)	2.88 (0.80)	6.47 (0.28)	8.81 (0.83)
MP	h_{MP} (%)	26	17	52	34
	A_{MP}^{80} (%)	21	14	44	27
	Mean MP (%)	13 (21)	11 (23)	20 (0.17)	19 (24)

Values in parentheses are standard deviations

was mainly caused by a longitudinal gradient ($h_{IC,D}$, 98.9%; $h_{IC,L}$, 55.9%). The spatial distribution of TN was very close to what was observed with the TOC, with a h_{TN} ranging from 85% in December to 98% in March. The higher h_P observed with TOC, IC, and TN suggests that these compounds were in excess in all sections of the lake, in contrast to CH_4 and DO. Moreover, while the processes involved in CH_4 and DO exhibited marked vertical gradients, the TOC, IC, and TN were more subject to longitudinal than vertical gradients, as previously observed in other aquatic ecosystems (Descloux et al. 2017).

To test the NHM with surface heat maps, we processed CH_4 flux data (F_{CH4}) previously reported by Gerardo-Nieto et al. (2017) from Lake Hambre. Figure S3 shows surface heat maps over three seasons, the corresponding NHM graphs and the parameters h_{FCH4}, A_{FCH4}^{80}, and λ_{FCH4}. In this case too, the model gave the standard asymptotic shape observed with C_{CH4} and C_{DO} in LG, but in this case with no λ_{FCH4}, except 2% observed during winter. It is noteworthy that, although the mean magnitude of F_{CH4} changed among seasons; i.e., 4.16, 23.04, and 1.55 mg m^{-2} day^{-1}, in spring, summer and winter, respectively, the corresponding h_{FCH4} were similar (Figure S3d), suggesting that, in contrast to h_{CCH4} observed in LG, the spatial homogeneity stayed constant over seasons; i.e., 78.3, 77.0, and 65.1%. Overall, these results confirm that, as expected, comparison of parameter distribution among seasons is possible using the NHM.

The NHM was also tested with depth-time maps of C_{DO} and C_{CH4} data, from the northeast section of LF, previously published (Sepulveda-Jauregui et al. 2018b). Figure 5a, b shows the heat maps generated from these data that were measured at the same position over 1 year at 0.5-m depth intervals. As in LG, a negative relationship was observed between C_{CH4} and C_{DO} in both depth and time, with higher C_{CH4} levels where lower DO concentrations were observed, and vice versa. The average C_{CH4} and C_{DO} over the entire depth-time map were 0.23 and 4.89 mg L^{-1}, respectively. In contrast to what was observed in LG, the CH_4/DO molar ratio over the entire water column and year was 0.095, i.e., up to two orders of magnitude below the ratio observed in LG, and below the theoretical ratio of 0.5 mol of CH_4 oxidized per mole of oxygen. Therefore, in LF, the CH_4/DO molar ratio indicated that DO was present in excess, in most of the water column. Consequently, in LF, C_{DO} was more homogeneously distributed than C_{CH4}, with h_{CDO}, A_{CDO}^{80}, and λ_{CDO} values of 60.0, 48.4, and 0.9%, respectively, in comparison with h_{CCH4}, A_{CCH4}^{80}, and λ_{CCH4} values of 14.3, 11.0, and 19.9%, respectively. This opposite pattern, compared to LG, is explained by the absence of a significant anoxic water column and by the excess of DO, compared to CH_4; i.e., low CH_4/DO molar ratio.

Single-dimension analysis in LG

As mentioned, the NHM allows the discrimination of longitudinal and depth distributions of any parameter and therefore to establish the main direction of heterogeneities. For example, when applied to the C_{DO} data for September in LG, the clear depth gradient observed at 200 m from the dam (Fig. 2a) was numerically confirmed by $h_{CDO,D}$, $A_{CDO,D}^{80}$,

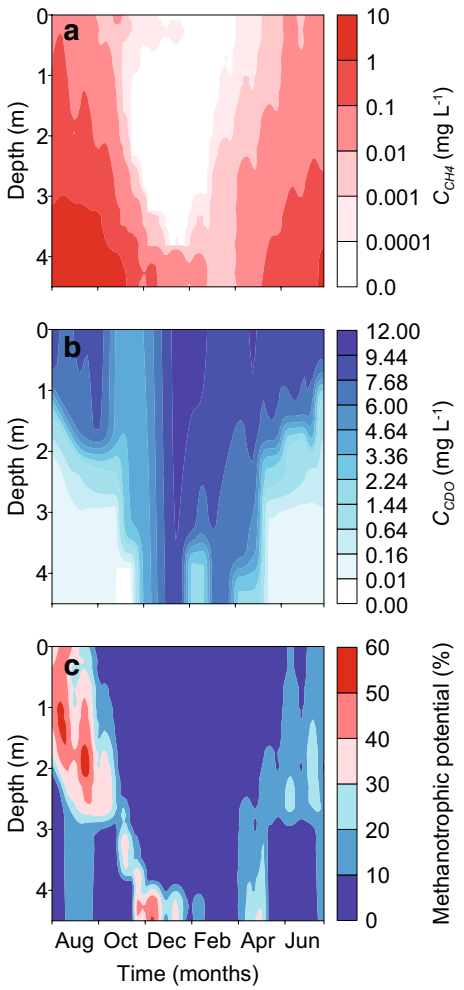

Fig. 5 Heat maps of the depth-time distributions of dissolved methane (C_{CH4}) (**a**), dissolved oxygen (C_{DO}) (**b**), and methanotrophic potential (**c**), in Lake Grosse Fuchskuhle (LF)

and $\lambda_{CDO,D}$, with values of 9.6, 8.2, and 80.6%, respectively, while the absence of a clear longitudinal gradient at 2-m depth was confirmed by $h_{CDO,L}$, $A^{80}_{CDO,L}$, and $\lambda_{CDO,L}$, with values of 94.2, 73.4, and 0.0%, respectively. In contrast, the depth distribution analysis of C_{CH4} in December, when mixing and small gradients were observed, showed that $h_{CCH4,D}$, $A^{80}_{CCH4,D}$, and $\lambda_{CCH4,D}$ were 94.9, 78.6, and 0.0%, respectively, at 200 m from the dam, while the longitudinal distributions were 68.6, 61.7, and 0.0% for $h_{CCH4,L}$, $A^{80}_{CCH4,L}$, and $\lambda_{CCH4,L}$, respectively, at 2-m depth. Therefore, in the latter case, C_{CH4} was subject to a stronger longitudinal gradient than depth gradient during mixing.

These longitudinal and depth profiles were used to determine the bidimensional simplified anisotropic vectors in LG; i.e., $\Omega_{P,L,D}$ and $\omega_{P,L,D}$. Figure 4e shows the results of these determinations for C_{CH4}, as well as the mean vector, determined from Eqs. (5) and (6), while Fig. 4f shows these same parameters for C_{DO}. Overall, $\Omega_{CDO,L,D}$ and $\omega_{CDO,L,D}$ were higher than $\Omega_{CCH4,L,D}$ and $\omega_{CCH4,L,D}$, respectively, which confirms that C_{DO} was more heterogeneously and anisotropically distributed. For both DO and CH_4, the mean $\omega_{P,L,D}$, were positive, indicating that the depth profiles were more heterogeneous than longitudinal profiles, and more evidently for C_{DO}. It is worthwhile to mention that $\omega_{CCH4,L,D}$ was negative in December, but not during the three other periods. The latter indicates that during most of the year the CH_4 distribution was dominantly controlled by stratification, more than by the lateral input of wastewater at the west of the lake. Contrastingly when mixing occurs, the lateral input of organic matter prevailed on the CH_4 distribution.

Multiparametric estimations for processes prediction

As previously mentioned, the NHM possesses a predictive capacity to establish the available habitat for a given process. As an example, we used C_{CH4} and C_{DO} data from LG to test the capability of the NHM to establish the methanotrophic potential. Figure 6 shows the vertical section maps of *MP* as well as the corresponding h_{MP}, $A^{\%}_{MP}$, and λ_{MP} (also presented in Table 1). Notably, this analysis showed that the methanotrophic potential was limited to only a small section of LG, as evidenced by a small $A^{\%}_{MP}$ and a large λ_{MP} (Fig. 6). Furthermore, this potential is, as expected from C_{DO} and C_{CH4} profiles, more heterogeneously distributed along depth profiles than longitudinal profiles. It should be noted that this analysis confirmed that CH_4 was in excess in most of the water column, compared to DO, as previously established. This was confirmed, first, by analyzing separately the proportionality parameters $C_{CH4}/(C_{CH4}+K_{S,CH4})$ and $C_{DO}/(C_{DO}+K_{S,DO})$, of the Monod model used to establish *MP*. This analysis showed that DO was more limiting than CH_4 in 75, 90, 54, and 69% of the lake section, in September, December, March and May, respectively. Additional evidence is the fact that h_{MP} and A^{80}_{MP} were positively correlated to h_{CDO} and A^{80}_{CDO} and inversely correlated to h_{CCH4} and A^{80}_{CCH4} (Table 1). We applied the same strategy in LF and determined that *MP* was also limited to a small fraction of the depth-time section (Fig. 5c). Overall, this *MP* analysis shows that NHM also allows to determine the section of a lake that is prone to harbor a given biological process, in complement to mapping that allows qualitative assessment of the latter.

Statistical analysis

The NHM also allows to guide field sampling campaigns. Since data distribution and homogeneity are unknown a priori, it is not possible to define the number of samples required to describe accurately the aquatic ecosystem. Therefore, it is not uncommon to determine the sampling

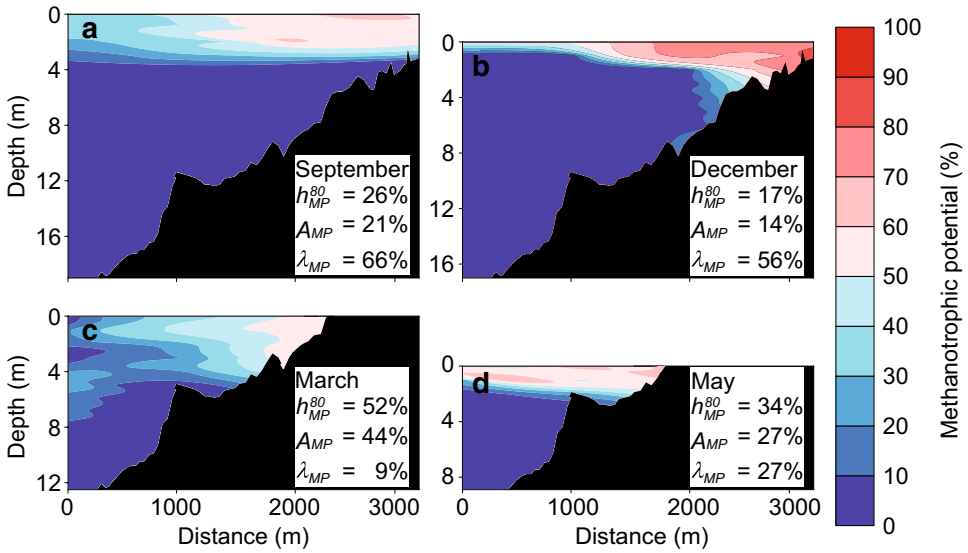

Fig. 6 Heat maps and NHM parameters of the methanotrophic potential in LG, in September (**a**), December (**b**), March (**c**) and May (**d**). Black area represents bathymetry data

density based on a two-step approach, the first being a qualitative/semiquantitative survey to detect areas of interest, and the second being the study itself. The statistical analysis of the first step can inform if the sampling procedure was adequate. To determine the adequacy of sampling procedures, we suggest using h_P as the characteristic parameter, as it reflects data distribution. Therefore, the impact of sampling density can be assessed through the relative absolute error on h_P ($E_{h,P}$), and sampling density can be modified by reducing artificially the number of depth or longitudinal measurements. If a given reduction of the sampling density results in little change of $E_{h,P}$ or in a $E_{h,P}$ below a given limit (e.g., 10%), the sampling strategy might be considered adequate. To illustrate that, we considered the interpolated matrix of C_{CH4} and C_{DO} in LG as the reference, and we determined $E_{h,P}$ for reduced datasets of depth or longitudinal measurements (Fig. S4). As observed, the impact on $E_{h,P}$ of reduced datasets, was highly dependent on the season and the studied parameter. Overall, $E_{h,CDO}$ was usually higher than $E_{h,CCH4}$, which can be easily explained by lower h_{CDO}, compared to h_{CCH4}. Similarly, in December, when h_{CDO} and h_{CCH4} were the lowest and the highest, respectively, the impact of reducing sampling density had the highest impact on $E_{h,CDO}$ and the lowest on $E_{h,CCH4}$.

Strengths and weaknesses of the model

Our numerical model is easily applicable with no specialized background on numerical methods and with slight computing effort. The model accurately describes the spatial and spatiotemporal distributions of any parameters by assigning a numerical value to homogeneity and other spatiotemporal attributes, which are otherwise qualitatively assessed. We have seen that the NHM allows to quantify homogeneity in two space–space or space–time dimensions but also in one space or time dimension, which in turn allows to compare them to establish a simplified vector of anisotropy. In addition to homogeneity, the NHM also establishes the fraction of the ecosystem that contains a given percentage of the total amount of a compound or parameter ($A_P^{\%}$), or in which no detectable levels of the measured parameter are found (λ_P). The NHM combined with a process model, also allows to establish the percentage of an ecosystem that is an appropriate habitat for a given process, as exemplified in this work with methanotrophy.

A comparison of the main attributes of the NHM and other simple statistic methods are listed in Table S1a. The primary and main objective of the NHM is the determination of h_P, which is in many ways similar to CV or MAD. Indeed, both h_P and CV or MAD parameters are assigning a numerical value to data dispersion. However, several differences exist between these parameters. First, as opposed to CV or MAD, h_P is based on weighted parameters; i.e. each parameter data is associated with a grid cell area (two-dimensions analysis) or length (one-dimension analysis). Therefore, except in the case of CV or MAD determined from regular grids, in which each measurement is equally weighted, h_P will be more representative of the ecosystem than CV or MAD. Second, in the NHM, h_P, $A_P^{\%}$, and λ_P, are normalized bounded parameters with a range of 0–100%, which facilitate comparison among ecosystems, as well as among periods of time or sections of a given ecosystem. Third, CV is based on root-mean-square deviations, which results in a more important weight assigned to outliers, and therefore over-represents them. This is not the case of the NHM, where each measurement is weighted only by the grid cell area or length, similarly to MAD, where each datum is equally weighted. To illustrate the latter, Figure S5 shows

a large impact of outliers on CV, and a limited effect on h_P and MAD. This is further illustrated in Figure S6, where data with the same mean and different distributions have a slight effect on h_P and MAD, whereas CV tends to be more variable.

Instead of a single CV or MAD analysis, a standard statistical analysis of data distribution often takes into account a combination of statistical parameters, including mean, variance, and CV for normally distributed data, or robust estimators such as median, geometric mean, MAD, interquartile range for non-normally distributed data. These multiple standard approaches may be an alternative or complement to NHM, with the purpose of establishing the central tendency and dispersion of the dataset. In this regard, it is worth mentioning that, when based on interpolated maps, the NHM model intrinsically includes standard statistical analysis during the interpolation step, automatically performed and based on several methods, the best of which is selected during data analysis; e.g., Surfer software, as used in the present work.

The NHM might be a simple but useful tool to better constrain aquatic ecosystems functioning. First, as observed in LG with C_{DO} and in LF with C_{CH4}, a low h_P, or $A_P^{\%}$, as well as a high λ_P, is a clear indicator of limiting conditions, meaning that the uptake of the measured compounds exceeds its availability. Contrarily, high h_P and low λ_P, are indicators of an excess of the measured compound. This was clearly observed with TOC, IC, and TN concentrations data in LG, not surprising as the lake receives large wastewater discharges. When combined, the h_P of two related compounds being inversely correlated, suggest a coupling between them, as observed for CH_4 and DO in LG and LF, both being coupled through aerobic methanotrophy. In LG, CH_4 was dominant over DO, while the opposite was observed in LF. Second, the NHM allows for a comparison of homogeneity among space–space or space–time dimensions, and to determine a simplified anisotropic vector. A radical case was C_{CH4} measured in December in LG, with a $\omega_{CCH4,L,D}$ of $-33.5°$. This angle means that the longitudinal gradient of C_{CH4} was by far superior to depth gradient, which is in agreement with the large discharge of wastewater at the west of the lake, promoting methanogenesis and flowing to the east, progressively diluted by mixing of the water column. On the contrary, C_{DO} measured in September in LG exhibited a $\omega_{CDO,L,D}$ of $+41.9°$, showing unequivocally that during stratification the biological processes involved in DO production/uptake are almost exclusively evident along a vertical axis. Hence, the comparison of homogeneity among different dimensions and the simplified anisotropic vector inform about the dominant axis along which the successions of biological processes take place and may help to establish the origin and fate of the compounds involved in a specific biogeochemical process. Third, the NHM allows for comparison among ecosystems or sections within one of them, and as such, might be adopted by other researchers, allowing to build a unified database of spatio-temporal variability in aquatic ecosystems, at a global scale.

Despite the strengths of the NHM, several weaknesses are worth mentioning. First, the NHM is based on an ordered cumulative function that loses the coordinates information related to each measurement. Thus, the model informs about, for instance, the percentage of the ecosystem section that contain a given percentage of a compound or that does not contain a significant level of it ($A_P^{\%}$ and λ_P), but the model fails in informing the location of these sections. Therefore, the NHM may advantageously be combined with a heat map to mitigate the loss of information. Similarly, the NHM parameters are scaled by the mean, which is a strength to allow for independent comparison among ecosystems but does not contain any magnitude information about the studied parameter. This can be solved by combining the NHM parameter with the mean, as usually done when reporting CV or standard deviation. In conclusion, the NHM might be a potential tool, easy to apply in combination with other methods, to better describe the high spatiotemporal variability in aquatic ecosystems. Since the model allows to combine several dimensions of different nature, h_P, $A_P^{\%}$, λ_P, $\Omega_{P,X,Y}$, and $\omega_{P,X,Y}$ can be used to quantify any combination of spatial and temporal variations, at any scale.

Acknowledgements We gratefully acknowledge Consejo Nacional de Ciencia y Tecnología (Conacyt), Mexico for financial support to Rodrigo Gonzalez-Valencia, Felipe Magana-Rodriguez, and Teresa Aguirrezabala-Campano (Grant nos. 266244, 419562, and 531383, respectively). We also thank Secretaría del Medio Ambiente y Recursos Naturales (Semarnat) for financial support received through project 23661, and Victoria T. Velázquez-Martínez, Juan Corona-Hernández, Francisco Silva-Olmedo, and David Flores-Rojas for technical assistance.

Compliance with ethical standards

Conflict of interest The authors declare that they have no conflicts of interest.

References

APHA (2012) Standard methods for the examination of water and wastewater, 22nd edn. American Public Health Association (APHA), American Water Works Association (AWWA), Water Environment Federation (WEF), Washington DC

Bagstad KJ, Semmens DJ, Ancona ZH, Sherrouse BC (2017) Evaluating alternative methods for biophysical and cultural ecosystem services hotspot mapping in natural resource planning. Landsc Ecol 32:77–97. https://doi.org/10.1007/s10980-016-0430-6

Bastviken D, Cole J, Pace M, Tranvik L (2004) Methane emissions from lakes: dependence of lake characteristics, two regional assessments, and a global estimate. Glob Biogeochem Cycl 18:GB4009. https://doi.org/10.1029/2004GB002238

Bellido JL, Tulonen T, Kankaala P, Ojala A (2013) Concentrations of CO_2 and CH_4 in water columns of two stratified boreal lakes during a year of atypical summer precipitation. Biogeochemistry 113:613–627. https://doi.org/10.1007/s10533-012-9792-2

Branco CWC, Kozlowsky-Suzuki B, Sousa-Filho IF, Guarino AWS, Rocha RJ (2009) Impact of climate on the vertical water column structure of Lajes Reservoir (Brazil): a tropical reservoir case. Lakes Reserv Res Manag 14:175–191. https://doi.org/10.1111/j.1440-1770.2009.00403.x

Delwiche KB, Hemond HF (2017) Methane bubble size distributions, flux, and dissolution in a freshwater lake. Environ Sci Technol 51:13733–13739. https://doi.org/10.1021/acs.est.7b04243

Descloux S, Chanudet V, Serca D, Guerin F (2017) Methane and nitrous oxide annual emissions from an old eutrophic temperate reservoir. Sci Total Environ 598:959–972. https://doi.org/10.1016/j.scitotenv.2017.04.066

Encinas Fernandez J, Peeters F, Hofmann H (2014) Importance of the autumn overturn and anoxic conditions in the hypolimnion for the annual methane emissions from a temperate lake. Environ Sci Technol 48:7297–7304. https://doi.org/10.1021/es4056164

Fraterrigo JM, Rusak JA (2008) Disturbance-driven changes in the variability of ecological patterns and processes. Ecol Lett 11:756–770. https://doi.org/10.1111/j.1461-0248.2008.01191.x

Geary RC (1954) The contiguity ratio and statistical mapping. Inc Stat 5(3):115–146. https://doi.org/10.2307/2986645

Gerardo-Nieto O, Astorga-Espana MS, Mansilla A, Thalasso F (2017) Initial report on methane and carbon dioxide emission dynamics from sub-Antarctic freshwater ecosystems: a seasonal study of a lake and a reservoir. Sci Total Environ 593–594:144–154. https://doi.org/10.1016/j.scitotenv.2017.02.144

Giling DP, Nejstgaard JC, Berger SA, Grossart HP, Kirillin G, Penske A, Lentz M, Casper P, Sareyka J, Gessner MO (2017) Thermocline deepening boosts ecosystem metabolism: evidence from a large-scale lake enclosure experiment simulating a summer storm. Glob Change Biol 23:1448–1462. https://doi.org/10.1111/gcb.13512

Gonzalez-Valencia R, Sepulveda-Jauregui A, Martinez-Cruz K, Hoyos-Santillan J, Dendooven L, Thalasso F (2014) Methane emissions from Mexican freshwater bodies: correlations with water pollution. Hydrobiologia 721:9–22. https://doi.org/10.1007/s10750-013-1632-4

Gonzalez-Valencia R, Magana-Rodriguez F, Cristobal J, Thalasso F (2016) Hotspot detection and spatial distribution of methane emissions from landfills by a surface probe method. Waste Manag 55:299–305. https://doi.org/10.1016/j.wasman.2016.03.004

Gustafson EJ (1998) Quantifying landscape spatial pattern: what is the state of the art? Ecosystems 1:143–156. https://doi.org/10.1007/s100219900011

He FL, LaFrankie JV, Song B (2002) Scale dependence of tree abundance and richness in a tropical rain forest, Malaysia. Landsc Ecol 17:559–568. https://doi.org/10.1023/A:1021514104193

Hofmann H (2013) Spatiotemporal distribution patterns of dissolved methane in lakes: how accurate are the current estimations of the diffusive flux path? Geophys Res Lett 40:2779–2784. https://doi.org/10.1002/grl.50453

Hofmann H, Federwisch L, Peeters F (2010) Wave-induced release of methane: littoral zones as a source of methane in lakes. Limnol Oceanogr 55:1990–2000. https://doi.org/10.4319/lo.2010.55.5.1990

Hutchinson GE, Löffler H (1956) The thermal classification of lakes. Proc Natl Acad Sci USA 42:84–86. https://doi.org/10.1073/pnas.42.2.84

Imboden DM, Wüest A (1995) Mixing mechanisms in lakes. In: Lerman A, Imboden DM, Gat JR (eds) Physics and chemistry of lakes. Springer, Berlin, pp 83–138

Jane SF, Rose KC (2018) Carbon quality regulates the temperature dependence of aquatic ecosystem respiration. Freshw Biol 63:1407–1419. https://doi.org/10.1111/fwb.13168

Kaizu Y, Iio M, Yamada H, Noguchi N (2011) Development of unmanned airboat for water-quality mapping. Biosyst Eng 109:338–347. https://doi.org/10.1016/j.biosystemseng.2011.04.013

Legendre P, Fortin MJ (1989) Spatial pattern and ecological analysis. Vegetatio 80:107–138. https://doi.org/10.1007/BF00048036

Li BL (1995) Wavelet analysis for characterizing spatial heterogeneity in the subsurface. In: Laine AF, Unser MA (eds) Proceedings of the society of photo-optical instrumentation engineers (SPIE). SPIE, Washington, pp 736–746

Martinez-Cruz K, Sepulveda-Jauregui A, Anthony KW, Thalasso F (2015) Geographic and seasonal variation of dissolved methane and aerobic methane oxidation in Alaskan lakes. Biogeosciences 12:4595–4606. https://doi.org/10.5194/bg-12-4595-2015

Matheron G (1963) Principles of geostatistics. Econ Geol 58(8):1246–1266. https://doi.org/10.2113/gsecongeo.58.8.1246

Meteored (2016) Histórico del Clima en Cuautitlán Izcalli. https://www.meteored.mx/cuautitlan-izcalli/historico. Accessed 24 May 2016

Moran PAP (1950) Notes on continuous stochastic phenomena. Biometrika 37:17–23

Murase J, Sakai Y, Kametani A, Sugimoto A (2005) Dynamics of methane in mesotrophic Lake Biwa, Japan. Ecol Res 20:377–385. https://doi.org/10.1007/s11284-005-0053-x

Padisák J, Barbosa F, Koschel R, Krienitz L (2003) Deep layer cyanoprokaryota maxima in temperate and tropical lakes. Adv Limnol 58:175–199

Pannard A, Bormans M, Lagadeuc Y (2008) Phytoplankton species turnover controlled by physical forcing at different time scales. Can J Fish Aquat Sci 65:47–60. https://doi.org/10.1139/F07-149

Rajala T, Redenbach C, Särkka A, Sormani M (2018) A review on anisotropy analysis of spatial point patterns. Spat Stat 28:141–168. https://doi.org/10.1016/j.spasta.2018.04.005

Rosenberg MS (2000) The bearing correlogram: a new method of analyzing directional spatial autocorrelation. Geogr Anal 32:267–278

Segers R (1998) Methane production and methane consumption: a review of processes underlying wetland methane fluxes. Biogeochemistry 41:23–51. https://doi.org/10.1023/A:1005929032764

Sepulveda-Jauregui A, Martinez-Cruz K, Strohm A, Anthony KMW, Thalasso F (2012) A new method for field measurement of dissolved methane in water using infrared tunable diode laser absorption spectroscopy. Limnol Oceanogr Methods 10:560–567. https://doi.org/10.4319/lom.2012.10.560

Sepulveda-Jauregui A, Hoyos-Santillan J, Gutierrez-Mendieta FJ, Torres-Alvarado R, Dendooven L, Thalasso F (2013) The impact of anthropogenic pollution on limnological characteristics of a subtropical highland reservoir "Lago de Guadalupe". Mexico. Knowl Manag Aquat Ecosyst. https://doi.org/10.1051/kmae/2013059

Sepulveda-Jauregui A, Hoyos-Santillan J, Martinez-Cruz K, Anthony KMW, Casper P, Belmonte-Izquierdo Y, Thalasso F (2018a) Eutrophication exacerbates the impact of climate warming on lake methane emission. Sci Total Environ 636:411–419. https://doi.org/10.1016/j.scitotenv.2018.04.283

Sepulveda-Jauregui A, Martinez-Cruz K, Lau M, Casper P (2018b) Assessment of methane and carbon dioxide emissions in two subbasins of a small acidic bog lake artificially divided 30 years ago. Freshw Biol 63:1534–1549. https://doi.org/10.1111/fwb.13182

Steinle L, Graves CA, Treude T, Ferre B, Biastoch A, Bussmann I, Berndt C, Krastel S, James RH, Behrens E, Boning CW, Greinert J, Sapart CJ, Scheinert M, Sommer S, Lehmann MF, Niemann H (2015) Water column methanotrophy controlled by a rapid oceanographic switch. Nat Geosci 8:378–382. https://doi.org/10.1038/Ngeo2420

Striegl RG, Michmerhuizen CM (1998) Hydrologic influence on methane and carbon dioxide dynamics at two north-central Minnesota lakes. Limnol Oceanogr 43:1519–1529. https://doi.org/10.4319/lo.1998.43.7.1519

Thah PH, Sitanggang IS (2016) Contextual outlier detection on hotspot data in Riau Province using k-means algorithm. In: 2nd international symposium on Lapan-Ipb Satellite (Lisat) for food security and environmental monitoring, vol 33, pp 258–268

Veldtman R (2005) The ecology of southern African wild silk moths (Gonometa Species, Lepidoptera: Lasiocampidae): consequences for their sustainable use. Dissertation, University of Pretoria

Wang JF, Zhang TL, Fu BJ (2016) A measure of spatial stratified heterogeneity. Ecol Indic 67:250–256. https://doi.org/10.1016/j.ecolind.2016.02.052

Watkins JM, Weidel BC, Rudstam LG, Holeckl KT (2015) Spatial extent and dissipation of the deep chlorophyll layer in Lake Ontario during the Lake Ontario lower foodweb assessment, 2003 and 2008. Aquat Ecosyst Health Manag 18:18–27. https://doi.org/10.1080/14634988.2014.937316

Weber UW, Cook PG, Brennwald MS, Kipfer R, Stieglitz TC (2019) A novel approach to quantify air–water gas exchange in shallow surface waters using high-resolution time series of dissolved atmospheric gases. Environ Sci Technol 53:1463–1470. https://doi.org/10.1021/acs.est.8b05318

Wik M, Crill PM, Varner RK, Bastviken D (2013) Multiyear measurements of ebullitive methane flux from three subarctic lakes. J Geophys Res Biogeosci 118:1307–1321. https://doi.org/10.1002/jgrg.20103

Willmott CJ, Matsuura K (2006) On the use of dimensioned measures of error to evaluate the performance of spatial interpolators. Int J Geogr Inf Sci 20:89–102. https://doi.org/10.1080/13658810500286976

Winder M, Hunter DA (2008) Temporal organization of phytoplankton communities linked to physical forcing. Oecologia 156:179–192. https://doi.org/10.1007/s00442-008-0964-7